Materials Chemistry and Physics 249 (2020) 123070

Contents lists available at ScienceDirect

Materials Chemistry and Physics

journal homepage: www.elsevier.com/locate/matchemphys

Surface adaptation prompted enhanced photo and thermoluminescence properties of Dy^{3+} doped wollastonite nanophosphor

T.B. Nijalingappa [a,b], M.K. Veeraiah [b,*], G.P. Darshan [c], D. Kavyashree [d], S.C. Sharma [e,f], H. B. Premkumar [g], H. Nagabhushana [h]

[a] Department of Chemistry, Sree Siddaganaga College of Arts, Science & Commerce, Tumkur, 572102, India
[b] Sri Siddhartha Academy of Higher Education, Tumkur, 572105, India
[c] Department of Physics, Acharya Institute of Graduate Studies, Bangalore, 560107, India
[d] Department of Physics, Acharya Institute of Technology, Bangalore, 560107, India
[e] National Assessment and Accreditation Council, Bangalore, 560 072, India
[f] Work Carried out as honorary Professor, Jain University, Bangalore, 562 112, India
[g] Department of Physics, M.S. Ramaiah University of Applied Sciences, Bangalore, 560 054, India
[h] Prof. C.N.R. Rao Centre for Advanced Materials, Tumkur University, Tumkur, 572 103, India

HIGHLIGHTS

- Novel SiO_2@$CaSiO_3$:Dy^{3+} (1–11 mol %) nanophosphors (NPs) were synthesized by simple solution combustion route.
- Photoluminescence (PL) and thermoluminescence (TL) properties of the prepared nanophosphors were extensively investigated.
- The photometric properties of the prepared samples clearly evident that NPs emits warm white color with high color purity.
- The present optimized nanophosphor was highly useful for display and dosimetry applications.

GRAPHICAL ABSTRACT

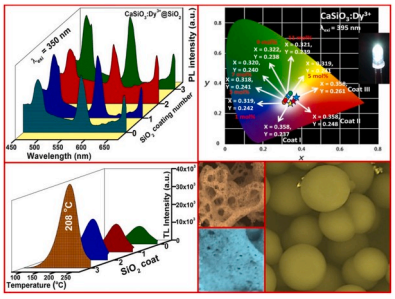

ARTICLE INFO

Keywords:
Solution combustion
Photoluminescence
Thermoluminescence
Photometric properties

ABSTRACT

The novel $CaSiO_3$:Dy^{3+} (1–11 mol %) nanophosphors synthesized via simple solution combustion route and covered with silica (SiO_2) by the Stöber method are reported in the present work. The X ray diffraction analysis verifies the phase purity of the synthesized samples. The diffraction peaks observed in the recorded powder x-ray diffraction patterns are in good relation with those known for the $CaSiO_3$ structure. The photoluminescence and thermoluminescence properties of SiO_2@$CaSiO_3$:Dy^{3+} (3 mol %) nanophosphors were extensively investigated. The 3-fold enhancement in the photoluminescence intensity of nanophosphors after surface coating was observed, that may be due to light diffraction and multiplied by shell SiO_2. The utility of the prepared samples in white light emitting diodes was confirmed by studying photometric properties. The thermoluminescence study of the samples with different γ-ray doses showed good linearity up to 4 kGy and, thereafter, the sub-linear behavior was noticed. The variation in the thermoluminescence intensity arises as a consequence of competition between different trapping centers. The aforementioned results signify that the present material was highly useful for display and dosimetry applications.

* Corresponding author.
E-mail address: veeraiahmk@gmail.com (M.K. Veeraiah).

https://doi.org/10.1016/j.matchemphys.2020.123070
Received 10 October 2019; Received in revised form 26 February 2020; Accepted 10 April 2020
Available online 11 April 2020

1. Introduction

In recent years, the morphology engineering has significant applications in various areas, including solar cells, imaging, catalytic, dosimetry, etc. [1–4]. Commonly, the nano/micron sized silica particles were used in core-shell materials because they are of uniform tunable sizes and less expensive than other materials [5,6]. The size and number of coatings of the nanophosphors (NPs) were well controlled by means of silica core. The silicate based hosts show promising luminescence behavior owing to their exceptional thermal, chemical, mechanical stability and structural diversity [7–11]. The exciting luminescence characteristics of the silicate-based host materials may be due to their energy storage tendency which can be capable of converting energy into light emission either by optical stimulation or thermal stimulation [12,13]. Further, the Dy^{3+} ions were extensively utilized as an activator in many efficient hosts in order to produce white light emission originated from the $^5D \rightarrow {}^4F$ transitions [14,15]. Till date, the silicate-based NPs were prepared by several routes, namely, the solid state reaction method, sol-gel, hydrothermal, solvothermal, solution combustion (SC), etc. [16–19]. Among them, the SC route was considered to be economical, least energy utilization and eco-friendly for the fabrication of various NPs [20,21]. The white light-emitting diodes (WLEDs) were considered as a next generation light sources that will replace the conventional incandescent and fluorescence lamps, because of its high luminous efficiency and lifetime, energy saving, eco-friendly, simple fabrication, enhanced stability and economic benefits [22–26]. The silica (SiO_2) covered NPs exhibit outstanding advantages, including high surface area, chemical stability, bio-compatibility, tunable pore size and shell thickness, high optical transparency, less toxicity, etc. Further, rich Si-OH groups offers significant wide range of applications, such as drug transport carriers, bio-imaging, luminescent probes in various fields, DNA sequencing, clinical diagnosing and immunoassaying [27,28]. Thermoluminescence dosimetry is a versatile technique for assessment of ionizing radiations (gamma, beta and X-rays), patient, personal and environmental dosimetry, dating of geological and archaeological samples. In addition, this method can also be probed lattice defects as well as trapping centers in large energy band gap NPs [29,30]. The key process involved in this technique is the light emission from heated samples, in which unconfined electrons were previously stored. These electrons recombine with holes, resulting in TL glow curves. The trapping parameters (activation energy, order of kinetics and frequency factor) can be clearly elucidates from the glow peak variation [31]. Herein, the photoluminescence (PL) and thermoluminescence (TL) properties of SiO_2@$CaSiO_3$:Dy^{3+} (1–11 mol %) NPs prepared via SC route were investigated in detail.

2. Experimental

2.1. Synthesis of SiO_2 particles by Stöber method

The well-known Stöber route was followed to synthesize the SiO_2 uniform spheres [32,33]. In the present work, tetraethyl orthosilicate

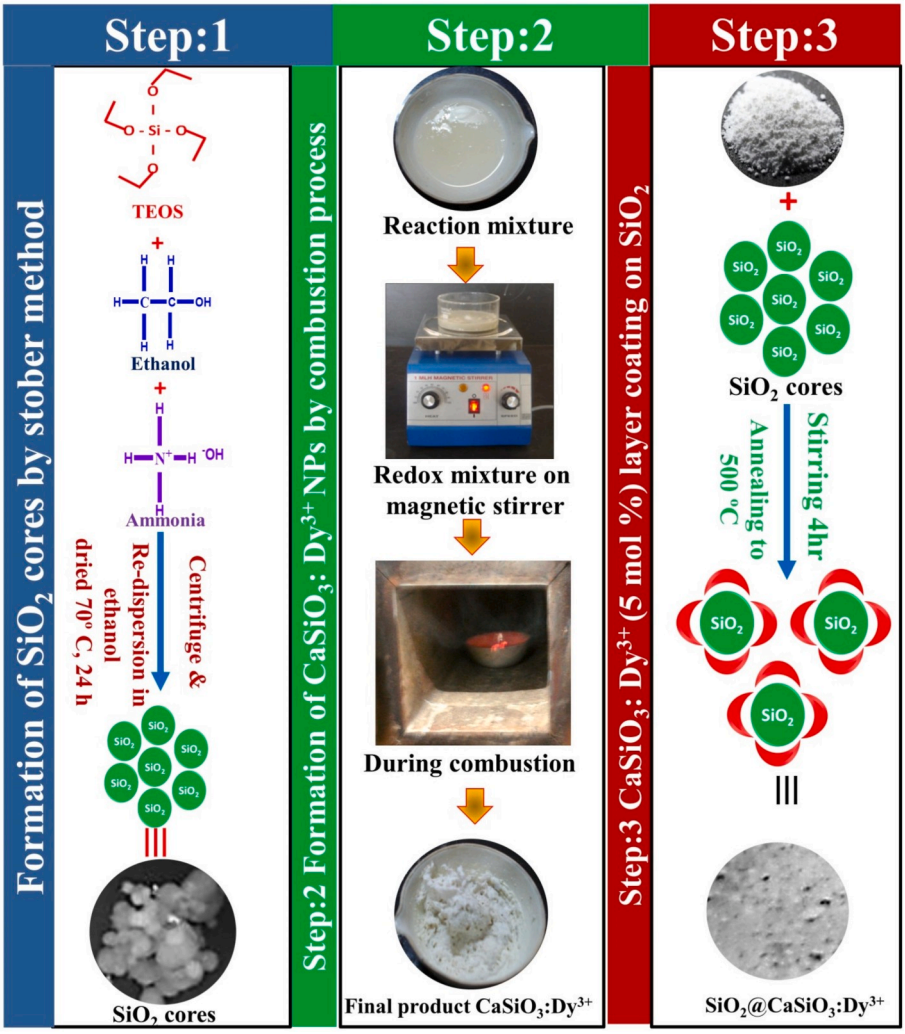

Fig. 1. Schematic to illustrate synthesis of SiO_2@$CaSiO_3$:Dy^{3+} (1–11 mol %) NPs.

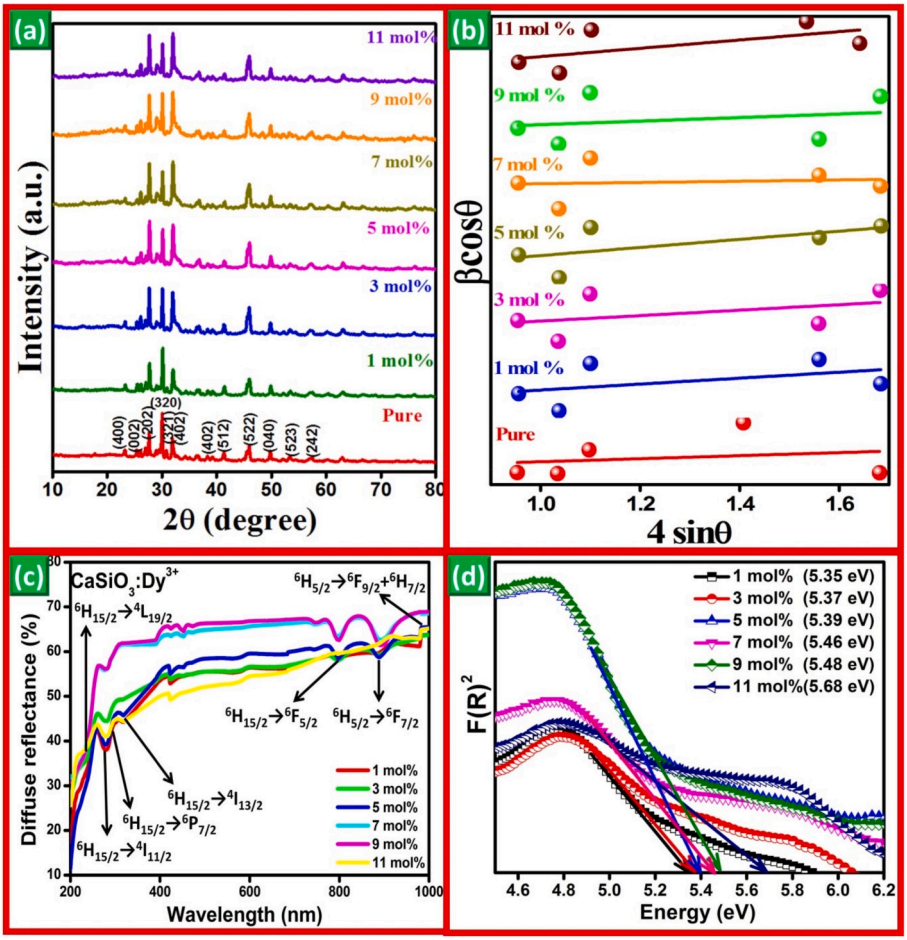

Fig. 2. (a) PXRD patterns, (b) W-H plots, (c) DR spectra and (d) energy band gap plots of $CaSiO_3:Dy^{3+}$ (1–11 mol %) NPs.

(TEOS, 99 wt %) was added into 42.4 mL ethanol solution of 5.4 ml double distilled H_2O and 29.4 mL NH_3*H_2O (25-28 wt %) to synthesize the SiO_2 particles. The obtained precipitate was centrifuged, washed with double distilled water and dried at ~80 °C for 20 h.

2.2. Synthesis of $CaSiO_3:Dy^{3+}$ NPs via solution combustion route

The simple SC route was employed to fabricate $CaSiO_3:Dy^{3+}$ (1–11 mol %) NPs. The analytical reagent (AR) grade Calcium nitrate tetrahydrate [Ca(NO3)2·4H2O; 99.99%, Sigma Aldrich], Dysprosium (III) nitrate hexahydrate [Dy(NO3)3.6H2O; 99.99%, Sigma Aldrich] and TEOS were used as starting materials and oxalyl dihydrazide was used as a fuel [ODH:$C_2H_6N_4O_2$] [34]. The appropriate quantities of calcium nitrate (11.099 g) and TEOS (11.18 mL) were mixed uniformly with distilled water using a probe sonicator. Further, various concentrations (1–11 mol %) of dysprosium nitrate were added to the above solution. The resulting reaction mixture was introduced into a preheated muffle furnace kept at 500 ± 10 °C. Initially, the precursor solution was dehydrated thermally and undergo auto-ignition of liberating gases. The final product was calcined at ~950 °C for 3 h and used for further studies.

2.3. Synthesis of $SiO_2@CaSiO_3:Dy^{3+}$ NPs

The phosphor coating with silica nanoparticles was performed via the sol-gel method. The proper amount of phosphor (10 g) was dispersed in a methanol (1 L) solution containing monodispersed silica nanoparticles for 2 h. The resulting phosphor powders were separated via centrifugation at a rotation speed of 3000 rpm for 20 min. Then, the phosphor powders were washed with deionized water several times and dried at 80 °C for 1 day. Similarly, different layers of coatings (I, II, III) were obtained by identically maintained the composition of the reaction mixture and reaction conditions, with the exception of the addition of phosphor. The resulting phosphor powders were recovered with the same procedures. The schematic diagram of the synthesis of $SiO_2@CaSiO_3:Dy^{3+}$ (1–11 mol %) NPs is shown in Fig. 1.

2.4. Characterization

The following tools were utilized for the characterization of the prepared samples; (i) Powder X-ray diffraction (PXRD): Shimadzu diffractometer (Model no −7000), (ii) Morphological and particle size analysis: Hitachi made (SEM, Model No.-TM 3000) and (TEM, Model No. H-8100), (iii) Diffuse reflectance (DR) measurements: PerkinElmer Spectrometer (Lambda-65) (iv) PL and TL studies: Horiba Fluorolog-3, modular Spectrofluorimeter and Nucleonix TLD reader.

3. Results and discussion

3.1. Powder X-ray diffraction (PXRD) analysis

The PXRD patterns of undoped and Dy^{3+} (1–11 mol %) doped $CaSiO_3$ NPs depicted in Fig. 2 (a). The diffraction profiles are in good relation to the monoclinic phase of $CaSiO_3$ (JCPDS No. 84-0655) [35]. No significant variations were noticed in profiles upon increase of Dy^{3+} concentration, and it indicates that the incorporation of Dy^{3+} ions does not alter the $CaSiO_3$ structure. In un-doped sample, the crystallization takes place along (320) plane, whereas, for doped samples, the crystallization

Table 1
Estimated crystallite size (D), micro-strain and lattice strain of prepared $CaSiO_3$: Dy^{3+} (1–11 mol %) NPs.

$CaSiO_3$: Dy^{3+} (mol %)	Crystallite size (nm)		Micro-strain ε (x 10^{-3})	Lattice strain ε (x10^{-3})
	Scherrer's method	W-H method		
1	31	43	1.11	3.19
3	31	39	1.09	3.47
5	31	42	1.12	3.29
7	30	31	1.15	4.39
9	33	35	1.11	3.89
11	30	41	1.02	2.24

proceeds along (202) and (402) planes. The decrease in intensity of (320) peak may be attributed to lattice distortion induced by the dopant.

The Scherrer relation and Williamson and Hall method were utilized for the elucidation of average crystallite sizes (D) and strain (ε), as follows [36]:

$$D = \frac{0.90\,\lambda}{\beta \cos\theta} \quad (1)$$

$$\beta \cos\theta = \varepsilon\,(4 \sin\theta) + \frac{\lambda}{D} \quad (2)$$

where β is the full width at half maximum in radian, λ is the X-ray wavelength (1.542 Å), and θ is the Bragg angle. Plotting graph between 4 sinθ along X – axis and βcosθ along Y – axis gives a straight line (Fig. 2 (b)). The slope and intercept of the straight line on the Y – axis gives the values of ε and D, respectively. The estimated values of ε and D for $CaSiO_3$: Dy^{3+} (1–11 mol %) NPs are tabulated in Table 1. The small changes in the obtained D values are attributed to neglected strain component in the Scherrer relation.

3.2. Diffuse reflectance (DR) studies

The DR spectra of $CdSiO_3$:Dy^{3+} (1–11 mol %) NPs are shown in Fig. 2 (c). The spectra exhibit many electronic absorption bands at ~322 nm ($^6H_{15/2} \rightarrow {}^4I_{11/2}$), ~350 nm ($^6H_{15/2} \rightarrow {}^6P_{7/2}$), ~364 nm ($^6H_{15/2} \rightarrow {}^4I_{13/2}$), ~381 nm ($^6H_{15/2} \rightarrow {}^6F_{5/2}$), ~796 nm ($^6H_{5/2} \rightarrow {}^6F_{7/2}$), and ~1071 nm ($^6H_{5/2} \rightarrow {}^6F_{9/2} + {}^6H_{7/2}$) related to the Dy^{3+} transitions [37]. The small red shifting of peaks was observed, which may due to the variations in the D values. The Kubelka-Munk theory was utilized for the calculation of the optical band gap (Eg) of NPs using the following equations [38]:

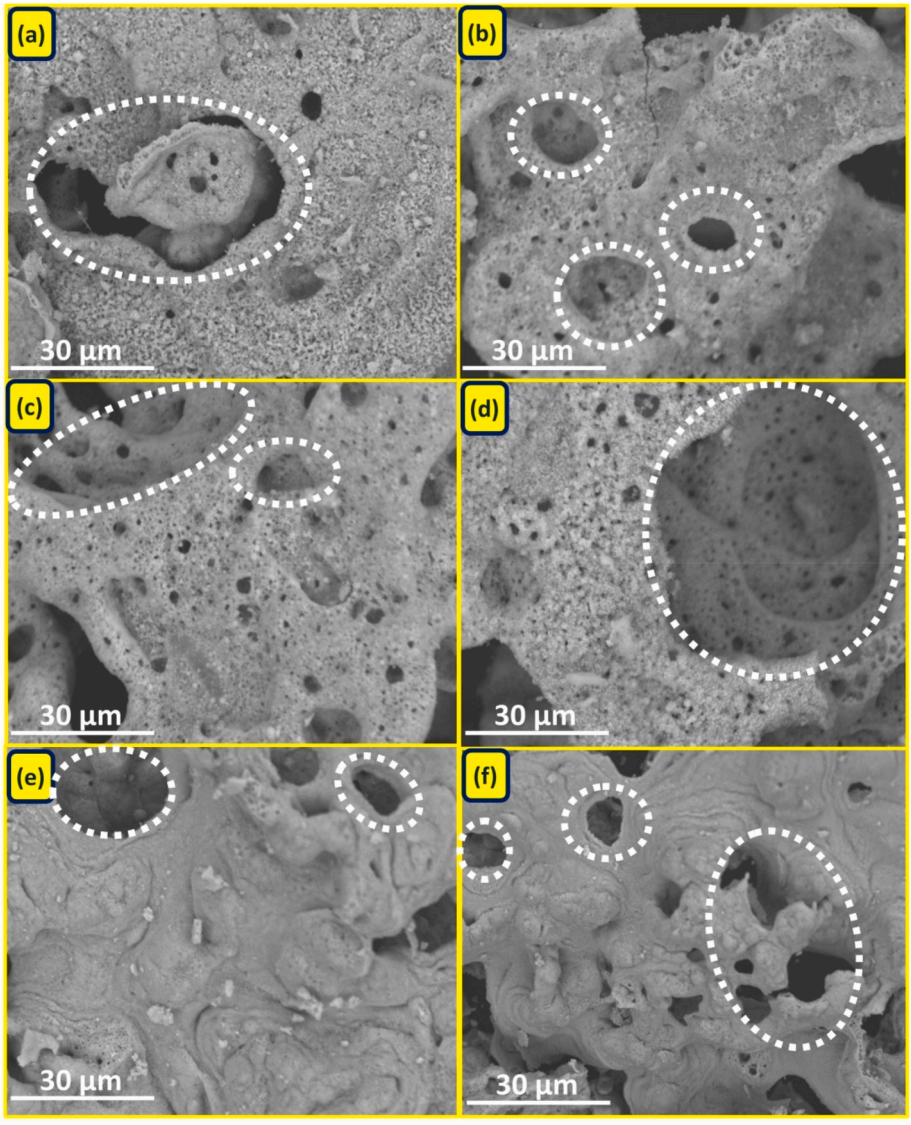

Fig. 3. SEM micrographs of $CaSiO_3$:Dy^{3+} (1–11 mol %) NPs.

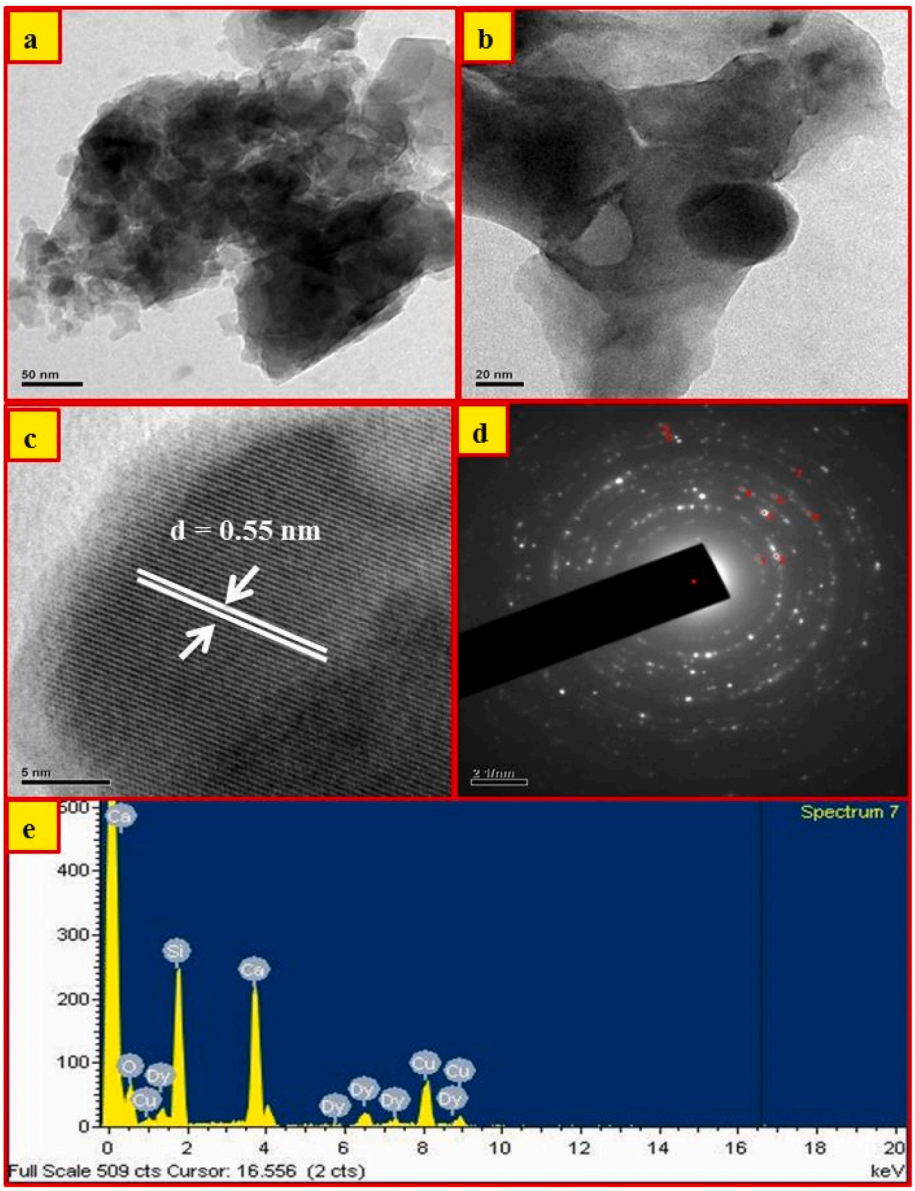

Fig. 4. (a & b). TEM, (c) HRTEM images, (d) SAED pattern and (e) EDAX spectra of $CaSiO_3:Dy^{3+}$ (5 mol %) NPs.

$$F(R_\infty) = \frac{(1-R_\infty)^2}{2R_\infty} \tag{3}$$

$$h\nu = \frac{1240}{\lambda} \tag{4}$$

where R_∞ is the reflection co-efficient and λ is the wavelength. The band gap plots of $CaSiO_3:Dy^{3+}$ (1–11 mol %) NPs are given in Fig. 2 (d). The Eg values were found to be in the range of 5.35–5.68 eV. The small variations in Eg values are noticed for the prepared samples, which may due to order or disorder structural changes appears from different experimental conditions.

3.3. Morphological studies

The SEM micrographs of $CaSiO_3:Dy^{3+}$ (1–11 mol %) NPs are shown in Fig. 3. It is seen that particles exhibit irregular shapes with a large number of pores and voids. The TEM images of $CaSiO_3:Dy^{3+}$ (5 & 9 mol %) NPs are shown in Fig. 4(a and b). The irregular and aggregated morphological structures are clearly noticed. From HRTEM image shown in Fig. 4 (c), the interplanar spacing (d) between was found to be ~0.55 nm. The SAED pattern of $CaSiO_3:Dy^{3+}$ (5 & 9 mol %) NPs clearly evidences the high crystallinity of the product and the (320), (202), (321) and (402) planes are well indexed (Fig. 4 (d)). The EDS spectrum of the $CaSiO_3:Dy^{3+}$ (5 mol %) NPs confirms the presence of Ca, Si, O and Dy^{3+} elements (Fig. 4 (e)).

The uniform spherical structure of core SiO2 is shown in Fig. 5 (a). However, $SiO_2@CaSiO_3:Dy^{3+}$ (C-I) exhibits dumbbell like structures (Fig. 5 (b)). When the CaSiO3:Dy3+ NPs coating was increased to II and III, the smooth surface structure with small pores is observed (Fig. 5(c, d)). The TEM images of $SiO_2@CaSiO_3:Dy^{3+}$ (5 mol %) with C-I & II coat NPs are shown in Fig. 5(e,f). It is evident in the images that core SiO2and $CaSiO_3:Dy^{3+}$ (5 mol %) can be easily identified. The continuous rings in the SAED pattern of NPs evidences the good crystallinity of the sample and they were well indexed to (522), (040), (522), (202), (402) and (320) planes of monoclinic $CaSiO_3$ (Fig. 5g). From the HRTEM pattern, the lattice spacing (d) was calculated to be ~0.58 nm (Fig. 5h).

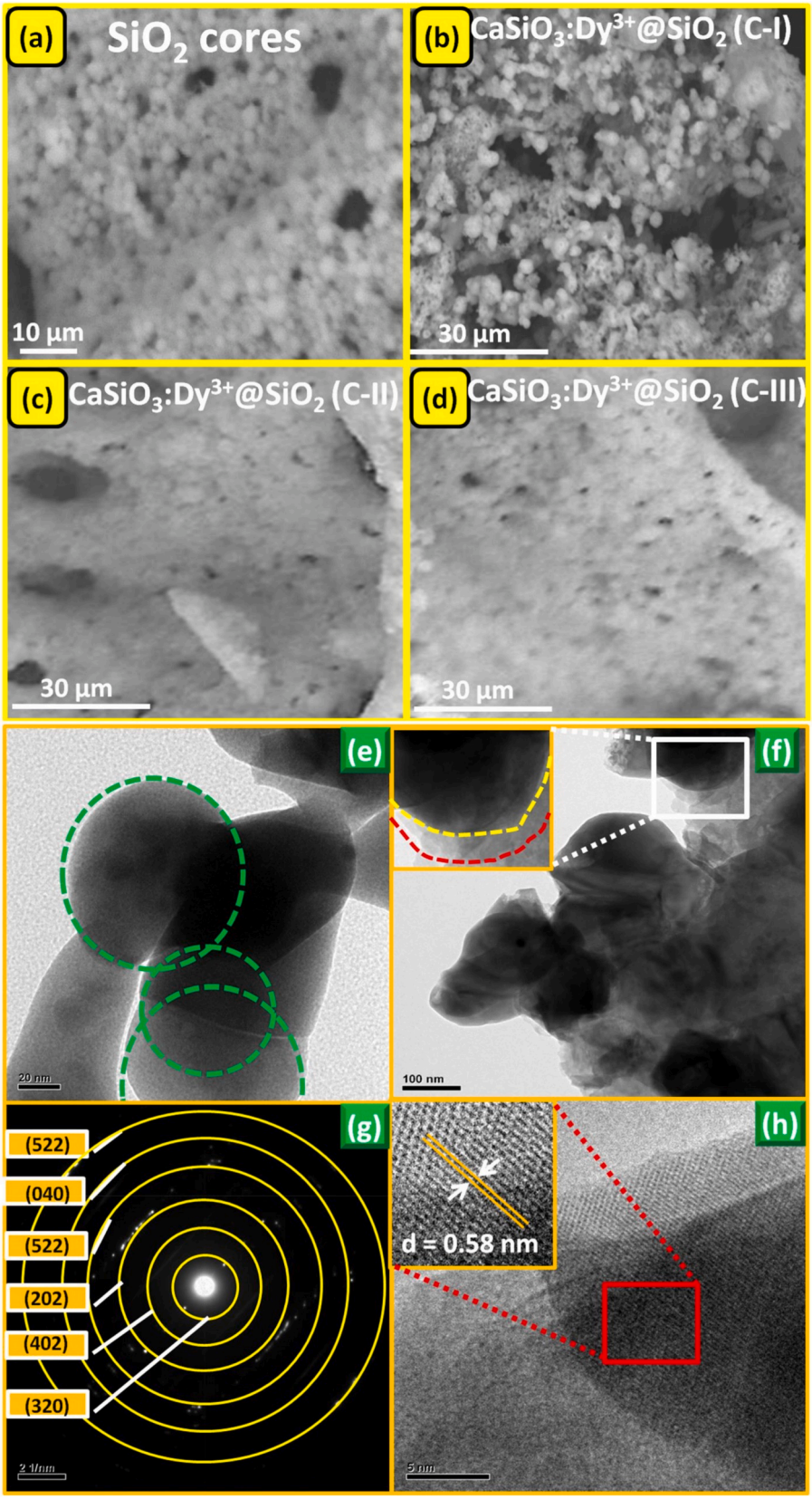

Fig. 5. (a-d). SEM images, (e,f) TEM images, (g) SAED patterns and (e) HRTEM of SiO_2@$CaSiO_3$:Dy^{3+} (1–11 mol %) NPs.

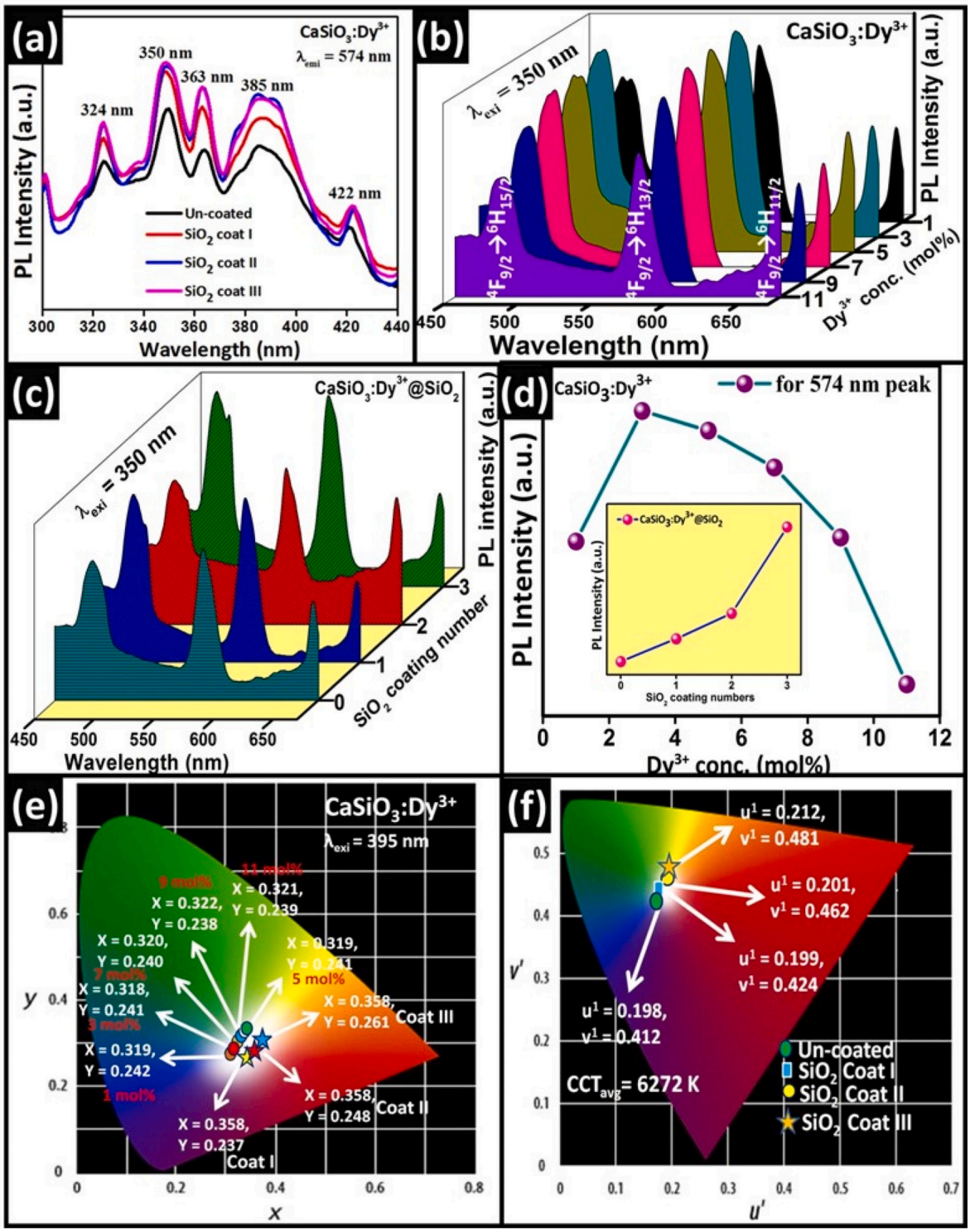

Fig. 6. (a) PL excitation spectra, (b) Emission spectra of $CaSiO_3$:Dy^{3+} (1–11 mol %) NPs, (c) Emission spectra of SiO_2@$CaSiO_3$:Dy^{3+} (1–11 mol %) NPs, (d) Plot of PL intensity v/s Dy^{3+} concentration, (e & f) CIE and CCT diagram of SiO_2@$CaSiO_3$:Dy^{3+} (1–11 mol %) NPs, respectively.

3.4. Photoluminescence (PL) properties

The PL excitation spectrum of SiO_2@$CaSiO_3$:Dy^{3+} (3 mol %) NPs with different coating levels upon λ_{Emis} = 574 nm is shown in Fig. 6 (a). The PLE spectrum consists of peaks at ~325, 350, 364, 387 and 423 nm, which are ascribed to the f-f transitions of Dy^{3+} ions [39]. Fig. 6 (b) represent the PL emission spectra of $CaSiO_3$:Dy^{3+} (1–11 mol %) NPs excited at 350 nm. The spectra exhibit intense characteristic peaks in the blue (~485 nm), yellow (~575 nm) and red (~666 nm) regions, which are attributed to the $^4F_{9/2}$→^6H_J (J = 15/2, 13/2 and 11/2) transitions of Dy^{3+} ions [40].

The effect of surface coatings on PL intensity was investigated in detail. The spectra of SiO_2@$CaSiO_3$:Dy^{3+} (3 mol %) NPs with different coating levels (without and with 1–3 coat) under λ_{Exc} = 350 nm are shown in Fig. 6 (c). The 3- fold enhancement in the PL emission intensity after surface coating was observed. The variation of PL emission

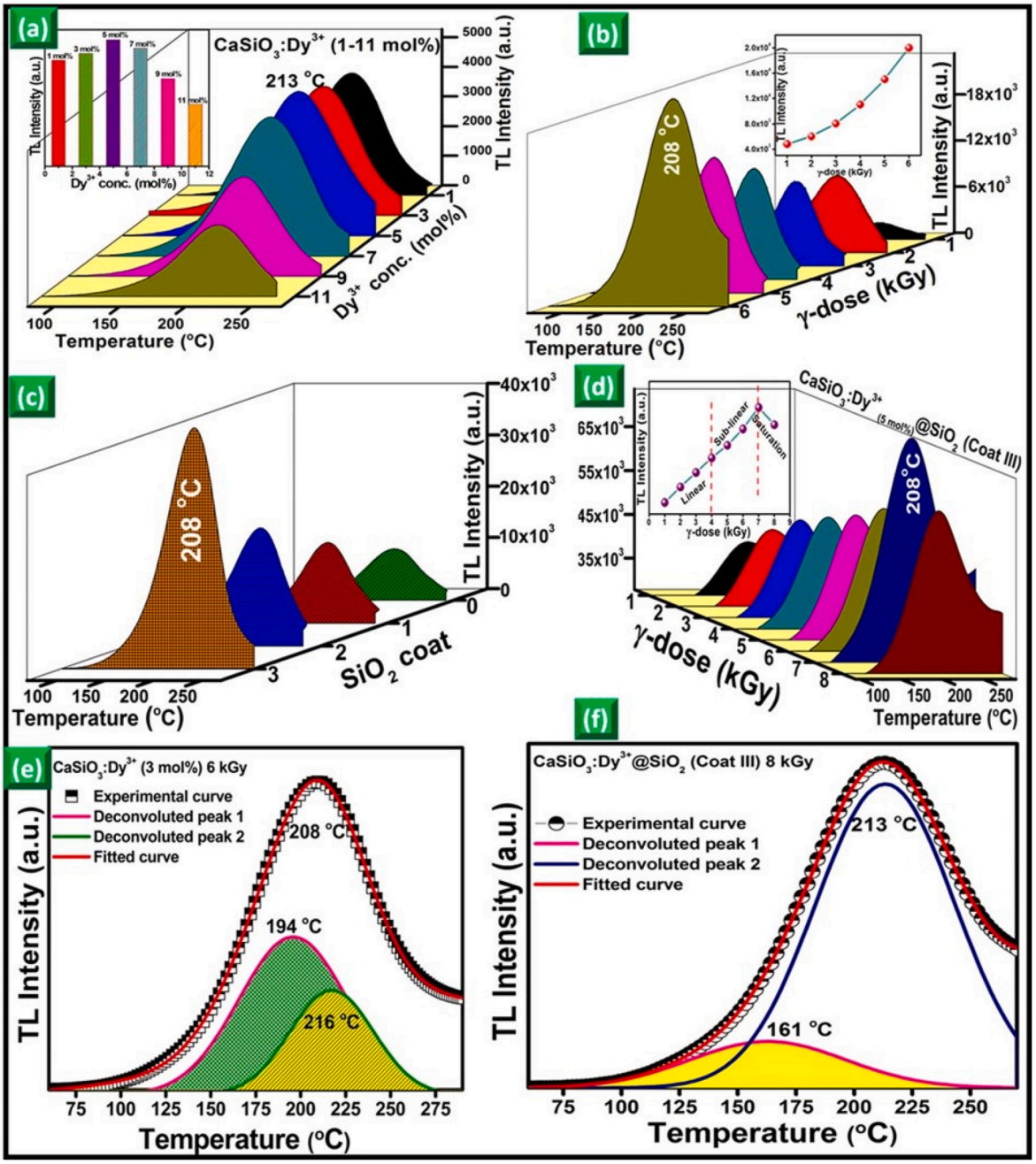

Fig. 7. TL glow curves of (a) $CaSiO_3:Dy^{3+}$ (1–11 mol %) NPs, (b) $CaSiO_3:Dy^{3+}$ (5 mol %) NPs under various gamma dose (1–6 kGy), (c) SiO_2@$CaSiO_3:Dy^{3+}$ (1–11 mol %) NPs, (d) SiO_2@$CaSiO_3:Dy^{3+}$ (1–11 mol %) NPs under various gamma dose (1–8 kGy), (e & f) Deconvoluted glow curves of coated and uncoated $CaSiO_3:Dy^{3+}$ (5 mol %) NPs.

intensity as a function of the SiO_2 coatings and Dy^{3+} concentration is shown in Fig. 6 (d). The maximal PL intensity is noticed for SiO_2 coated NPs (coat 4).

The variation of PL intensity was owing to well-known concentration quenching phenomena. The concentration quenching may be attributed to the energy transfer between two neighboring Dy^{3+} ions. According to Dexter theory, the critical distance between dopant ions can be estimated using the following relation [41]:

$$R_c \approx 2\left[\frac{3V}{4X_c\pi\ N}\right]^{1/3} \quad (5)$$

Where V is the unit cell volume, Xc is the critical concentration of dopant ions, Nis the number of ions per unit cell. In the present case, N = 4, V = 786 $(Å)^3$ and Xc = 0.03. The value of Rc was estimated to be ~10.2 Å. The obtained value of Rc is greater than 5 Å, and it indicates that the multipolar-multipolar interaction is noticeable for concentration quenching.

The International Commission on Illumination (CIE) coordinate values of the prepared samples were estimated by using the emission spectra recorded under the 350 nm excitation. The estimated chromaticity coordinates (x, y) are found in the white domain of the CIE chromaticity diagram (Fig. 6 (e)). In addition, the correlated color temperature (CCT) ((Fig. 6 (e)) values and color purity (CP) were calculated using the relations described in the literature [42]. The average CCT and CP values were found to be ~6272 K and 88%. The results clearly evidenced the possible use of the phosphors in WLEDs applications.

Table 2
Kinetic parameters (E, s) of $CaSiO_3:Dy^{3+}$ (1–11 mol %) NPs by various methods.

Method	Peak 1		Peak 2		Peak 3		Peak 4	
	E(eV)	s (s^{-1})	E(eV)	s (s^{-1})	E(eV)	s (s^{-1})	E(eV)	s (s^{-1})
Peak shape	0.91	3.97 E+18	0.62	1.21 E+20	0.83	5.52 E+10	2.37	1.10 E+16
VHR	0.67	1.65 E+11	0.75	3.60 E+12	1.06	1.77 E+13	1.24	1.78 E+20
TLAnal Program	0.76	9.10 E+08	0.54	6.04 E+04	0.89	1.51 E+07	1.73	3.85 E+13
Graphical	0.89	1.19 E+09	1.11	3.26 E+13	1.57	1.09 E+08	1.86	2.54 E+12
CGCD	0.89	9.19 E+10	0.55	1.72 E+05	0.72	3.69 E+05	1.87	3.63 E+14

3.5. Thermoluminescence (TL) studies

The TL glow curves of $CaSiO_3:Dy^{3+}$ (1–11 mol %) NPs are given in Fig. 7 (a). The glow curves contain a broad peak at ~213 °C. The effect of Dy^{3+} concentration on TL intensity is shown in the inset of Fig. 7 (a). The shape of TL spectral curves remains the same, however, the increment of intensity is noticed up to 5 mol % and thereafter it decreases. The concentration quenching phenomena were responsible for such intensity diminishing nature. In Fig. 7 (b), the TL glow curves are shown for optimized $CaSiO_3:Dy^{3+}$ (5 mol %) NPs at different γ-ray dose (1–6 kGy). The spectra exhibit a broad and intense glow peak at 208 °C. A small shift in the peak position with different γ-ray doses is clearly noticed. The variation in TL intensity with different γ-doses is shown in the inset of Fig. 7 (b) and the linear increment in the TL intensity with increase of γ-dose was observed. Such increment in the TL intensity is appeared due to the surface defect generation upon γ-ray dose.

The TL glow curves of $SiO_2@CaSiO_3:Dy^{3+}$ (3 mol %) NPs with various coatings (1-3) recorded at 1 kGy γ-ray dose are shown in Fig. 7 (c). No obvious change in the shape are two-fold enhancement in the glow intensity are clearly observed. The maximum TL intensity curve was observed for $SiO_2@CaSiO_3:Dy^{3+}$ (3 mol %) NPs with coat (3). In Fig. 7 (d), the TL response of the 3 coated $SiO_2@CaSiO_3:Dy^{3+}$ (3 mol %) NPs is shown as a function of γ-ray dose. A broad, intense peak centered at ~208 °C is clearly obtained. Also, a linear increment in the TL intensity up to 4 kGy is noticed. However, the noticeable sub-linear/saturation nature with further increase of γ-ray dose is observed in the inset of Fig. 7 (d). Such variation in the TL intensity was arises as a consequence of creation of the more defects and overlapping of defect centre takes place, which has no contribution to the additional TL output.

The glow curves were deconvoluted using Gaussian fit method (Fig. 7 (e, f)) and the kinetic parameters were estimated [30]. In addition, the following relation was utilized to estimate geometric form factor (μ_g):

$$\mu_g = \frac{T_2 - T_m}{T_2 - T_1} \tag{6}$$

where, T_m is the maximum T_L temperature, T_1 and T_2 are the full width at half maximum temperatures. Further, the activation energy was also determined using Chen's method as described in the literature [43–47]. Further, frequency factor was estimated using the following relation:

$$\frac{\beta E}{kT_m^2} = s \exp\left(\frac{-E}{kT_m}\right)[1 + (b-1)\Delta_m] \tag{7}$$

where β is the linear heating rate and b is the order of kinetics. The kinetic parameters of the prepared samples are estimated and they are listed in Table 2. The trap depth of the deconvoluted peaks is obtained to be ~0.57 and 1.38 eV. The effect of heating rate (3–9 °C/s) on TL glow curves is systematically studied and it is given in Fig. 8 (a). The linear increase of TL intensity and peak shift towards higher temperature with increase of heating rate (3–9 °C/s) are noticed. The variation in the TL glow curve intensity and peak position can be explained by the fact that at lower heating rates the charge carriers have sufficient time and were migrating towards their combination centre results in re-trapping.

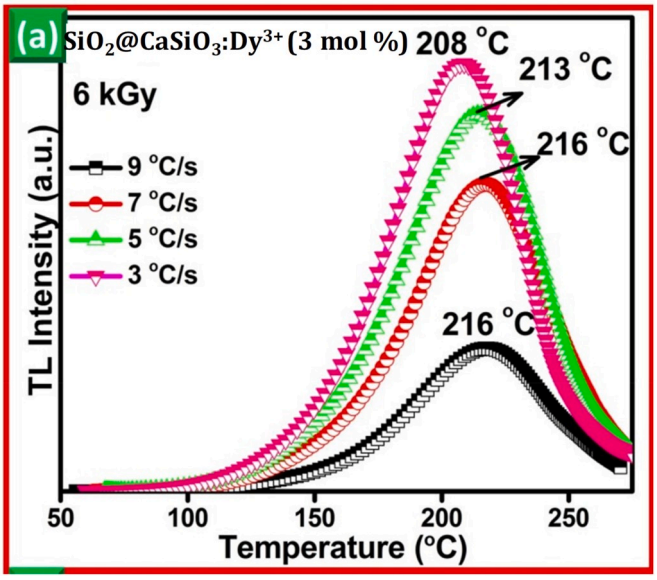

Fig. 8. TL glow curves of $CaSiO_3:Dy^{3+}$ (5 mol %) NPs (a) under various heating rate (3–9 °C/s).

Hence, these charge carriers were not responsible for actual luminescence.

4. Conclusions

Novel $SiO_2@CaSiO_3:Dy^{3+}$ (1–11 mol %) NPs were prepared via SC route using ODH as a fuel. The diffraction profiles endorse the monoclinic phase of $CaSiO_3$ (JCPDS No. 84-0655). The noticed variations in the Eg values (5.35–5.68 eV) may be due to order/disorder structural changes arises from various experimental conditions. The PL emission spectra consist of the peaks in blue (~485 nm), yellow (~575 nm) and red (~666 nm) regions, which are attributed to the transitions $^4F_{9/2} \rightarrow {}^6H_J$ (J = 15/2, 13/2 and 11/2) of Dy^{3+} ions. The 3- fold enhancement in the PL emission intensity after surface coating was noticed. The studied photometric properties (CIE, CCT and CP) evidenced its possible use in WLEDs applications. The linear increment in the TL intensity with increase of γ-dose was due to generation of surface defects upon γ-ray dose. The kinetic parameters, namely, activation energy, form factor and frequency factor, were estimated using Chen method. The aforementioned results open a new avenue of the prepared samples for display devices and dosimetry applications.

Declaration of conflict of interest

We declare that we do not have any commercial or associative interest that represents a conflict of interest in connection with the work submitted.

CRediT authorship contribution statement

T.B. Nijalingappa: Methodology, Investigation, Writing - original draft. **M.K. Veeraiah:** Supervision, Writing - review & editing. **G.P. Darshan:** Formal analysis. **D. Kavyashree:** Methodology, Investigation. **S.C. Sharma:** Supervision, Writing - review & editing. **H.B. Premkumar:** Formal analysis, Software, Data curation. **H. Nagabhushana:** Supervision.

References

[1] N. Rajamanickam, S.S. Kanmani, K. Jayakumar, K. Ramachandran, J. Photochem. Photobiol., A 378 (2019) 192–200.
[2] Victor V. Atuchin, Aleksandr S. Aleksandrovsky, Bair G. Bazarov, Jibzema G. Bazarova, Olga D. Chimitova, Yuriy G. Denisenko, Tatyana A. Gavrilova, Alexander S. Krylov, Eugene A. Maximovskiy, Maxim S. Molokeev, Aleksandr S. Oreshonkov, Alexey M. Pugachev, Nikolay V. Surovtsev, J. Alloys Compd. 785 (2019) 692–697.
[3] Lyubov Dyshlyuk, Olga Babich, Svetlana Ivanova, Natalya Vasilchenco, Victor Atuchin, Ilya Korolkov, Dmitriy Russakov, Prosekov Alexander, Int. Biodeterior. Biodegrad. 146 (2020) 104821.
[4] V.V. Atuchin, A.S. Aleksandrovsky, O.D. Chimitova, T.A. Gavrilova, A.S. Krylov, M. S. Molokeev, A.S. Oreshonkov, B.G. Bazarov, J.G. Bazarova, J. Phys. Chem. C 118 (28) (2014) 15404–15411.
[5] Deyu Kong, Haiwen Pan, Linhai Wang, David J. Corr, Jiansong Sheng, Cement Concr. Compos. 98 (2019) 137–149.
[6] Seongjun Moon, Kyung Jin Lee, Adv. Powder Technol. 28 (2017) 2914–2920.
[7] Joanne J. Rogers, Kenneth J.D. MacKenzie, William J. Trompetter, Gregory Rees, John V. Hanna, J. Non-Cryst. Solids 460 (2017) 98–105.
[8] Zhiguo Xia, Yuanyuan Zhang, Maxim S. Molokeev, Victor V. Atuchin, Yi Luo, Sci. Rep. 3 (2013) 3310.
[9] Zhiguo Xia, Yuanyuan Zhang, Maxim S. Molokeev, Victor V. Atuchin, J. Phys. Chem. C 117 (40) (2013) 20847–20854.
[10] Yi Wei, Chun Che Lin, Zewei Quan, Maxim S. Molokeev, Victor V. Atuchin, Ting-Shan Chan, Yujun Liang, Jun Lin, Guogang Li, RSC Adv. 6 (2016) 57261–57265.
[11] M. Venkataravanappa, H. Nagabhushana, B. Daruka Prasad, G.P. Darshan, R. B. Basavaraj, G.R. Vijayakumar, Ultrason. Sonochem. 34 (2017) 803–820.
[12] R.B. Basavaraj, H. Nagabhushana, G.P. Darshan, B. Daruka Prasad, M. Rahul, S. C. Sharma, R. Sudaramani, K.V. Archana, Dyes Pigments 147 (2017) 364–377.
[13] Ide Yusuke, Satoshi Tominaka, Taiki Okuyama, Nao Tsunoji, Dmitri Golberg, Nano Energy 59 (2019) 162–168.
[14] Esra Öztürk, Erkul Karacaoglu, Erdem Uzun, J. Lumin. 204 (2018) 51–58.
[15] Ding-Dian Xu, Wei Zhou, Ze Zhang, Shu-Jing Li, Xin-Rui Wang, Opt. Mater. 89 (2019) 197–202.
[16] M. Venkataravanappa, H. Nagabhushana, G.P. Darshan, S.C. Sharma, K. V. Archana, R.B. Basavaraj, B. Daruka Prasad, Mater. Res. Bull. 97 (2018) 281–292.
[17] Qiushi Wang, Yifu Zhang, Tao Hu, Xuyang Jing, Changgong Meng, Microporous Mesoporous Mater. 246 (2017) 102–113.
[18] M. Venkataravanappa, R.B. Basavaraj, G.P. Darshan, B. Daruka Prasad, S. C. Sharma, P. Hema Prabha, S. Ramani, H. Nagabhushana, J. Rare Earths 36 (2018) 690–702.
[19] V.B. Bhatkar, S.K. Omanwar, S.V. Moharil, Opt. Mater. 29 (2007) 1066–1070.
[20] G.P. Darshan, H.B. Premkumar, H. Nagabhushana, S.C. Sharma, S.C. Prashantha, B. Daruka Prasad, J. coll. int. sci. 464 (2016) 206–218.
[21] D. Prakashbabu, H.B. Ramalingam, R. Hari Krishna, B.M. Nagabhushana, S. Ponkumar, J. Lumin. 192 (2017) 496–503.
[22] G. Ramakrishna, H. Nagabhushana, K. Hareesh, D.V. Sunitha, Solid State Sci. 69 (2017) 56–63.
[23] B. Sundarakannan, M. Kottaisamy, Ceram. Int. 44 (2018) 14518–14522.
[24] Haipeng Ji, Zhaohui Huang, Zhiguo Xia, Maxim S. Molokeev, Victor V. Atuchin, Minghao Fang, Saifang Huang, Inorg. Chem. 53 (10) (2014) 5129–5135.
[25] Haipeng Ji, Le Wang, Maxim S. Molokeev, Naoto Hirosaki, Rongjun Xie, Zhaohui Huang, Zhiguo Xia, M. Otmar, ten Kate, Lihong Liu, Victor V. Atuchin, J. Mater. Chem. C 4 (28) (2016) 6855–6863.
[26] L. Julius, Leaño Jr., Shin-Ying Lin, Agata Lazarowska, Sebastian Mahlik, Marek Grinberg, Chaolun Liang, Wuzong Zhou, Maxim S. Molokeev, Victor V. Atuchin, Yi-Ting Tsai, Chun Che Lin, Hwo-shuenn Sheu, Ru-Shi Liu, Chem. Mater. 28 (19) (2016) 6822–6825.
[27] A. Sandhyarani, M.K. Kokila, G.P. Darshan, R.B. Basavaraj, B. Daruka Prasad, S. C. Sharma, T.K.S. Lakshmi, H. Nagabhushana, Chem. Eng. J. 327 (2017) 1135–1150.
[28] K.N. Venkatachalaiah, H. Nagabhushana, G.P. Darshan, R.B. Basavaraj, B. Daruka Prasad, Sensor. Actuator. B Chem. 251 (2017) 310–325.
[29] Yunxiu Ma, Zhangru Chen, Yingbo Chu, Yu Yang, Luyun Yang, J. Lumin. 204 (2018) 104–109.
[30] Nilo F. Cano, T.K. Gundu Rao, Jorge S. Ayala-Arenas, Carlos D. Gonzales-Lorenzo, Shigueo Watanabe, J. Lumin. 205 (2019) 324–328.
[31] M. Mangalagowri, R.B. Basavaraj, G.P. Darshan, M.S. Raju, H. Nagabhushana, Opt. Mater. 92 (2019) 125–135.
[32] Rui Liu, Yao-Wen Yeh, Vivienne H. Tam, Fengli Qu, Nan Yao, Rodney D. Priestley, Chem. Commun. 50 (2014) 9056–9059.
[33] Y.S. Chung, M.Y. Jeon, C.K. Kim, Ind. Eng. Chem. Res. 48 (2009) 740–748.
[34] G.P. Darshan, H.B. Premkumar, H. Nagabhushana, S.C. Sharma, B. Daruka Prasad, S.C. Prashantha, Dyes Pigments 134 (2016) 227–233.
[35] R.B. Basavaraj, G.P. Darshan, B. Daruka Prasad, S.C. Sharma, H. Nagabhushana, J. Rare Earths 37 (2019) 32–44.
[36] H.S. Sudheendra, G.P. Darshan, R.B. Basavaraj, Yashwanth V. Naik, M.K. Kokila, Opt. Mater. 90 (2019) 159–171.
[37] M. Dhanalakshmi, H. Nagabhushana, G.P. Darshan, R.B. Basavaraj, B. Daruka Prasad, J. Sci.: Adv. Mat. Dev. 2 (1) (2017) 22–33.
[38] G.P. Darshan, H.B. Premkumar, H. Nagabhushana, S.C. Sharma, B. Umesh, R. B. Basavaraj, Mater. Sci. Eng. C 99 (2019) 282–295.
[39] D. Navami, G.P. Darshan, R.B. Basavaraj, S.C. Sharma, D. Kavyashree, K. N. Venkatachalaiah, H. Nagabhushana, J. Photochem. Photobiol. Chem. 389 (2020) 112248.
[40] A.S. Rajashekharaiah, G.P. Darshan, H.B. Premkumar, P. Lalitha, S.C. Sharma, H. Nagabhushana, Mater. Chem. Phys. 242 (2020) 122468.
[41] A.S. Rajashekharaiah, G.P. Darshan, R.B. Basavaraj, Yashwanth V. Naik, D. Kavyashree, S.C. Sharma, H. Nagabhushana, Opt. Mater. 95 (2019) 109237.
[42] C.J. Shilpa, R.B. Basavaraj, G.P. Darshan, H.B. Premkumar, S.C. Sharma, H. Nagabhushana, J. Photochem. Photobiol. Chem. 376 (2019) 288–304.
[43] C. Suresh, H. Nagabhushana, G.P. Darshan, R.B. Basavaraj, H.J. Amith Yadav, Arabian J. Chem. 11 (2018) 460–482.
[44] N.J. Shivaramu, B.N. Lakshminarasappa, K.R. Nagabhushana, Fouran Singh, H. C. Swart, J. Lumin. 209 (2019) 179–187.
[45] Y. Zhao, Y. Wang, H. Jin, L. Yin, P.D. Townsend, J. Alloys Compd. 797 (2019) 1338–1347.
[46] H.B. Premkumar, D.V. Sunitha, H. Nagabhushana, S.C. Sharma, R.P.S. Chakradhar, J. Alloys Compd. 591 (2014) 337–345.
[47] S. Yashodamma, G.P. Darshan, R.B. Basavaraj, Udayabhanu, H. Nagabhushana, Opt. Mater. 92 (2019) 386–398.